CrossMark

Performance of ZnO synthesized by sol-gel as photocatalyst in the photooxidation reaction of NO

E. Luévano-Hipólito[1] · A. Martínez-de la Cruz[1] · E. López Cuéllar[1]

Abstract ZnO samples were prepared by sol-gel method applying a factorial design in order to improve the photocatalytic properties of the semiconductor oxide in the NO photooxidation reaction. The concentrations of zinc acetate and ammonium hydroxide were selected as critical variables in the synthesis of ZnO. Nine samples of ZnO were obtained as product of the factorial design and were characterized by X-ray powder diffraction, scanning electron microscopy, transmission electron microscopy, diffuse reflectance spectroscopy, and N_2 adsorption-desorption isotherms. The photocatalytic activity of ZnO samples was associated with the physical properties developed by each sample according to its respective conditions of synthesis. Some photocatalytic reaction parameters, such as mass of photocatalyst, irradiance, and relative humidity, were modified in order to evaluate its effect in the photocatalytic conversion of NO. As a relevant point, the relative humidity played an important role in the increase of the selectivity of the NO photooxidation reaction to innocuous nitrate ions when ZnO was used as photocatalyst.

Keywords ZnO · Sol-gel · Heterogeneous photocatalysis · NO_x

✉ A. Martínez-de la Cruz
azael70@yahoo.com.mx

[1] CIIDIT, Facultad de Ingeniería Mecánica y Eléctrica, Universidad Autónoma de Nuevo León, Ciudad Universitaria, C.P. 66451 San Nicolás de los Garza, N.L., Mexico

Introduction

Nitrogen oxides (NO_x) emitted from stationary and mobile sources are the origin of various health and environmental problems, such as irritated eyes, headache, pulmonary emphysema, acid rain, acidification of aquatic systems, ozone depletion, and photochemical smog (Bloh et al. 2014). Due to high NO_x concentration usually observed in big cities, efficient techniques for NO_x removal from the ambient environment are required. In this sense, heterogeneous photocatalysis is a clean and efficient technology to eliminate pollutants from the air (Lasek et al. 2013; Lyu et al. 2014; Verbruggen 2015).

So far, the titanium oxide TiO_2 has been widely studied as photocatalyst (Toma et al. 2004; Takeuchi et al. 2009; Nakata and Fujishima 2012); but in recent years, ZnO has attracted the attention due to its excellent optical and electrical properties. Zinc oxide (ZnO) is a semiconductor material of direct transition with a wide energy band gap ($E_g > 3.1$ eV). This property as well as its high bond energy (226 KJ·mol^{-1}) and high thermal and mechanical stability at room temperature make it attractive for its use in electronic devices, optoelectronics, and laser technology (Bacaksiz et al. 2009; García Núñez et al. 2014). On the other hand, ZnO oxide exhibits the crystalline structure of wurtzite at room temperature with useful electric properties (Baruah and Dutta 2009). Therefore, this oxide is widely used in mechanical actuators, piezoelectric sensors, and solar cells with high efficiency (Zhang et al. 2014; Hu et al. 2016).

The most common method to prepare powders of ZnO is by the precipitation of organic or inorganic salts in basic medium. Other processes have been successfully used in order to produce ZnO powders such as mechanochemical synthesis, emulsions, microemulsions, and thermal decomposition (Radzimska and Jesionowsky 2014; Moezzi et al. 2014; Kontopoulou et al. 2016). But beyond the simplicity of the

precipitation method to prepare ZnO, some negative aspects should be taken into account. For example, the synthesis by precipitation in basic medium of ZnO must be accompanied by a thermal treatment to remove reaction impurities, leading to the agglomeration of the particles during the formation of the oxide. As an interesting alternative, the synthesis of ZnO by sol-gel method is of special interest because the oxide is formed at lower temperatures than the traditional methods, avoiding the agglomeration of particles promoted by the use of high temperatures of synthesis. In addition, during the course of the sol-gel reaction, some experimental variables can be modified to obtain ZnO powders with physical properties that promote a higher photocatalytic activity, such as low particle size, high surface area, and a specific morphology.

In the field of heterogeneous photocatalysis in gaseous phase and specifically in the photooxidation reaction of NO_x, there are only few studies performed with ZnO (see Table 1). In general, the nitric oxide conversion degree by using ZnO as photocatalyst prepared by precipitation method in the presence of structuring agents has not reached more than 70 % (Huang et al. 2013; Wei et al. 2013; Kowsari and Bazri 2014; Luévano-Hipólito and Martínez-de la Cruz 2016). For example, Huang et al. have studied the activity of ZnO with different morphologies in the removal of NO_x gases. They found that ZnO with a sunflower morphology showed a higher photocatalytic activity under UV light irradiation when compared with the commercial TiO_2 P-25 Degussa, despite having a smaller value of surface area. The high photocatalytic activity of ZnO was associated with its hyperbranched nature and a larger number of oxygen vacancies on its surface. Wei et al. have also investigated the photocatalytic activity of ZnO spheres in the NO photooxidation reaction with visible radiation at 510 nm. The activation of ZnO with visible light was justified due to the presence of impurities of residual carbon in the sample. On the other hand, Kowsari et al. have found a maximum degree of NO conversion of 23 % using ZnO particles with flower-like morphology (Kowsari and Bazri 2014). As a common feature of these works, the synthesis of ZnO was assisted with complex organic compounds with the difficulty that it implies. On the other hand, Pei and Leung have studied the photocatalytic activity of the composite TiO_2–ZnO synthesized by sol-gel assisted with electrospinning method reaching an NO conversion degree of 80 % (Pei and Leung 2014). They have attributed their good results to a decreasing in the value of band gap of TiO_2 by the introduction of ZnO, which promotes the generation of electron hole pair and the generation of oxygen vacancies. However, the above results are difficult to compare because different operational conditions were used in all of them, i.e., inlet NO concentration, residence time, type of irradiation, and others.

Undoubtedly, the method employed to prepare ZnO induces the development of specific physicochemical properties

Table 1 Previous works on the photooxidation of NO using ZnO as photocatalyst

Synthesis	Raw materials	Morphology	Surface area ($m^2 \cdot g^{-1}$)[1]	Experimental conditions	NO conversion[2] (%)	Reference
Precipitation in the presence of structural and accelerant reagents	Zn(NO₃)₂·6H₂O (CH₂)₆N₄ C₂H₇NO	Spindle, sunflower, dandelion, and disk	39	450 W mercury lamp	55	Huang et al. (2013)
Carbon template and hydrated salt-assisted solvothermal method	Zn(NO₃)₂·6H₂O (CH₂)₆N₄ Na₃C₆H₅O₇	Spheres	607	Initial concentration 1 ppm of NO; 50 % RH; 450 W mercury lamp	70	Wei et al. (2013)
Hydrothermal method in presence of chiral ionic liquid	Zn(O₂CCH₃)₂ NaOH [TBA]₂[L-Tar]	Roses	33	0.1 g of photocatalyst; initial concentration 1 ppm of NO; 40 % RH	20	Kowsari and Bazri (2014)
Sol-gel assisted with electrospinning[3]	TTIP Zn(O₂CCH₃)₂ CH₃COOH	Fibers	45	300 W tungsten halogen lamp (720 ± 10 µW·cm⁻²); initial concentration 0.25 ppm of NO; 10–70 % RH	80	Pei and Leung (2014)
Precipitation, hydrothermal, and sol-gel method	Zn(NO₃)₂·6H₂O Zn(O₂CCH₃)₂ NH₄OH	Agglomerates and bars	16	Initial concentration 1 ppm of NO; UV lamp (8.2 W·m⁻²); 10–70 % RH; 50 mg of photocatalyst	70	Luévano-Hipólito and Martínez-de la Cruz (2016)

[1] Maximum surface area

[2] Maximum NO conversion reached

[3] TiO_2–ZnO composite

in the material to carry out successfully the photocatalytic oxidation of nitric oxide. From the works described in the Table 1, a specific morphology of particles of ZnO and the generation of oxygen vacancies were the important factors to reach a relatively high photocatalytic activity.

In a previous work, we found that the sol-gel method provides the optimal physical properties in ZnO to obtain the highest NO conversion degree compared with hydrothermal and precipitation methods (Luévano-Hipólito and Martínez-de la Cruz 2016). In the present work, the synthesis of ZnO was carried out by sol-gel method, but the concentrations of zinc acetate and ammonium hydroxide were modified in order to check its effect in the physical properties of the material, and consequently, in its photocatalytic activity. The samples were tested as photocatalysts in the NO photooxidation reaction and their activities were associated with the physicochemical properties developed during the sol-gel synthesis. Beyond the assessment of the photocatalytic activity of ZnO samples for the photooxidation reaction of NO, the selectivity of the ZnO to produce innocuous NO_3^- ions as final product of reaction was revised.

Experimental

Synthesis of ZnO

ZnO samples were synthesized by sol-gel method using a factorial design of the type 3^n ($n = 2$) to study the effect of two experimental variables in the final physical properties of the oxide. The reagents employed in the synthesis were zinc acetate ($Zn(CH_3COO)_2 \cdot 2H_2O$, DEQ, 99 %), ammonium hydroxide (NH_4OH, DEQ, 26 %), anhydrous ethanol (CH_3CH_2OH, DEQ, 99 %), and deionized water (H_2O). In a

typical experiment, two solutions were prepared. In the first one, different amounts of zinc acetate were dissolved in 50 mL of ethanol under magnetic stirring for 30 min. For the second solution, NH_4OH was dissolved in deionized water. After that, the ammonia solution was added dropwise into the zinc acetate solution under vigorous stirring for 1 h and then it was aged for 24 h at room temperature. The obtained gel in each case was dried at 70 °C for 24 h to promote the evaporation of the solvent and the formation of a solid white, which was used as precursor of ZnO. This material was heated in air at 300 °C for 24 h to remove the reaction of by-products and to induce the formation of ZnO with the crystalline structure of wurtzite. For the factorial design, the software Minitab™ was used, which provides a randomized order to make the synthesis of nine samples derived from the 3^n design. Table 2 shows the experimental conditions to synthesize the ZnO samples modifying the concentrations of Zn acetate and ammonium hydroxide.

Characterization

The structural characterization of ZnO samples was carried out by X-ray powder diffraction using a Bruker D8 Advance diffractometer with Cu K_α radiation (40 kV, 30 mA). A typical run was made with a 0.05° of step size and a dwell time of 0.5 s. The half-width of the strongest line in the diffraction patterns was measured to estimate the crystal size of the ZnO samples with spherical shape. Taking this data, the size of crystallite was calculated using the Scherrer equation. The morphology of the samples was analyzed by scanning electron microscopy and transmission electron microscopy using a FEI Nova NanoSEM 200 and an FEI Titan G2 80-300 microscopes with an accelerating voltage of 30 and 300 kV, respectively. The UV–Vis diffuse reflectance absorption spectra

Table 2   Physical properties of ZnO samples prepared by the sol-gel method

ZnO sample	NH$_4$OH (M)	Zinc precursor (M)	Crystal size (nm)	Particle size[1] (nm)	Band gap (eV)	Surface area (m^2·g^{-1})
E-1	8.2	0.20	–	L = 180, D = 36	3.28	13.1
E-2	2.0	0.20	–	L = 130, D = 42	3.29	16.0
E-3	0.8	0.02	42	35	3.26	26.9
E-4	8.2	0.02	41	32	3.25	27.3
E-5	2.0	0.10	69	45.5	3.26	14.2
E-6	8.2	0.10	–	L = 191, D = 38	3.27	13.1
E-7	0.8	0.10	–	L = 200, D = 37	3.27	9.0
E-8	0.8	0.20	–	D = 34[2], L = 166, D = 39[3]	3.27	16.7
E-9	2.0	0.02	26	47	3.26	29.8
ZnO-com	–	–	104	260	3.10	4.5

[1] Average value

[2] Semispherical particles

[3] Bars

of the samples were taken in an Agilent Technologies UV–Vis–NIR spectrophotometer model Cary 5000 series equipped with an integrating sphere. The BET surface area measurements were carried out by N_2 adsorption-desorption isotherms by means of a Bel-Japan Minisorp II surface area and pore size analyzer. The isotherms were evaluated at −196 °C after a pretreatment of the samples at 100 °C for 24 h.

Photocatalytic experiments

The photocatalytic activity of ZnO samples was tested in the photooxidation reaction of NO under UV irradiation, using a continuous flow reactor designed according with the ISO 22197-1. The photocatalytic reactor was made of stainless steel with a volume of 0.8 L and was equipped with an integrated window in its superior part to allow the pass of UV radiation. The photocatalyst was deposited over an area of 0.08 m^2 of a glass substrate with the help of a brush to disperse 50 mg of the photocatalyst in 5 mL of ethanol. With inlet gas, a stable mixture of 3 ppm of NO in N_2 was utilized. The concentration of inlet gas was adjusted to 1 ppm in NO by using synthetic air (20.5 vol% O_2 and 79.5 vol% N_2) and the flow rate of gas was adjusted to 1 L.min^{-1}. The source of UV irradiation were two fluorescent black lamps (TecnoLite) of 20 W, each one emitting mainly between 365 and 400 nm. The UV intensity in the center of the photocatalytic reactor was 8.2 W·m^{-2}, and it was measured with a UV light radiometer 290–390 nm (MANNIX 340 nm). The concentration of nitric oxide was continuously measured with a chemiluminescent NO analyzer (EcoPhysics CLD88p) with a sampling rate of 0.5 L.min^{-1}. The amount of nitrate and nitrite ions produced was followed by the analysis of 50 mL of deionized water used in the washed of the photocatalyst after the photocatalytic reaction. For this purpose, powders of the photocatalyst were sonicated in water for 30 min in order to desorb nitrates and nitrites and then it was centrifuged to obtain a crystalline solution. The concentration of nitrates ions in solution was measure in a Hach colorimeter trough the reduction of nitrate to nitrite ions by using cadmium as catalyst, while the nitrite ions concentration was determined by the diazotization method.

Results and Discussion

Characterization

The ZnO samples synthesized by sol-gel method were characterized structurally by X-ray powder diffraction and their diffractograms are shown in Fig. 1. It can be seen that all diffraction lines were in agreement with the corresponding lines of ZnO wurtzite according with the database JCPDS Card No. 36-1451, indicating that the samples were obtained in pure form at the level of resolution of the X-ray diffraction technique. From the analysis of the X-ray powder diffraction (XRD) patterns, differences were observed in all the samples in the crystallinity and in the crystallite size obtained by the Scherrer equation. This calculation was only carried out for the samples E-3, E-4, and E-9 because the coefficient $K = 0.9$ from the Scherrer equation must only be applied for

Fig. 1 X-ray powder diffraction patterns of ZnO samples prepared by the sol-gel method
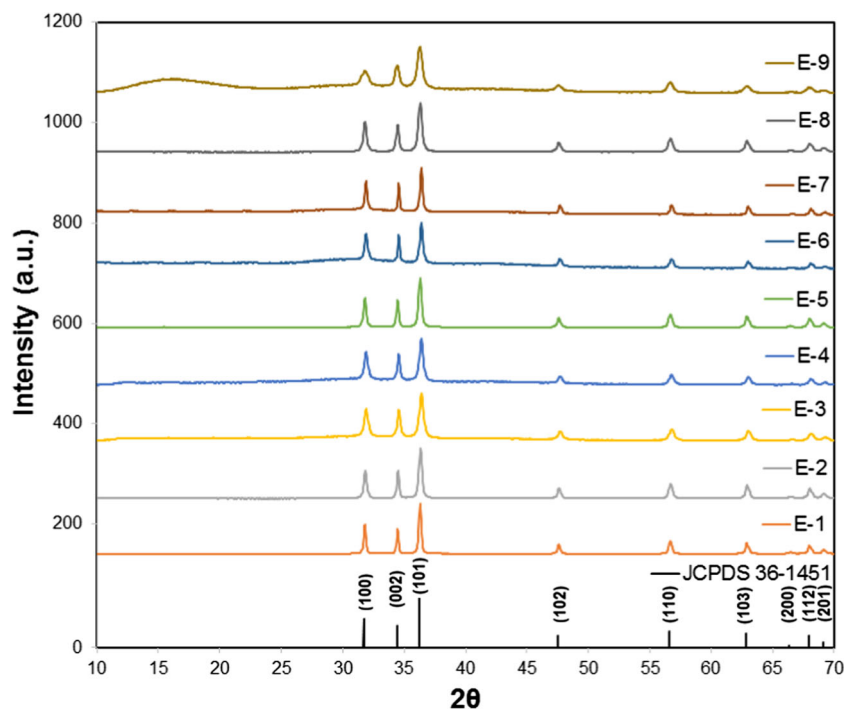
crystallites with spherical shapes (see Table 2). According to the profile of the XRD patterns, a low concentration of zinc acetate (0.02 M) promoted the formation of crystals with small sizes (E-3, E-4, and E-9). In this sense, the driving force for nucleation and growth of ZnO crystals was the supersaturation of the aqueous medium. A low concentration of zinc acetate produces a decrease in the supersaturation of the medium, and consequently, promotes an increasing in the critical radius value of ZnO particles ($r*$). This radius determines the maximum value to dissolve the particles and represents also the size at which the growth of the particles is favorable. This relation is expressed by equation (1), where S is the supersaturation of the medium, γ is the free energy required to generate one unit of surface area, k_B is the Boltzmann constant, T is the temperature, and Ω is the volume occupied by a formula unit in the particle nucleus (Cademartiri and Ozin 2010).

$$r^* = \frac{2\Omega\gamma}{k_B T \ln S} \tag{1}$$

As the zinc acetate is consumed during the crystal growth, S causes an increase in $r*$. The increasing in $r*$ implies a low growth rate, and therefore, the formation of particles with small size (Peng et al. 1998).

Diffuse reflectance spectra of ZnO samples were analyzed by UV–Vis spectroscopy in the range of 200 to 800 nm. All the samples absorbed below 400 nm, indicating that the activation was given by the absorption of UV radiation of the electromagnetic spectrum, as can be seen in Supplementary Fig. S1. From the emission spectrum of the UV lamp used, it can be seen that it provides the required energy to excite the solid semiconductor and thus produce the electron hole pair necessary to start the oxidation of the NO molecule. The energy band gap values obtained for the ZnO samples were similar between them, whose values ranged from 3.25 to 3.29 eV (see Table 2).

The N_2 adsorption-desorption isotherms of the nine ZnO samples showed a similar behavior as is shown in Supplementary Fig. S2. The profile of the adsorption-desorption curves corresponds with the type II according with the isotherm classification, which is associated with a weak interaction between the sample surface and adsorbate (N_2). This behavior is typical of a material nonporous (Condon 2006). The specific surface area values obtained for ZnO samples are shown in Table 2. These values vary between 9 and 30 $m^2.g^{-1}$. In general, the samples prepared with the lowest concentration of zinc acetate developed the highest surface area values (>26 $m^2 g^{-1}$), which is in accord with the small crystallite size calculated for these samples (E-3, E-4, and E-9). On the other hand, the relationship between surface area and NH_4OH concentration was not as evident as the relationship found with the zinc acetate.

The morphology of ZnO samples was analyzed by scanning electron microscopy (SEM). In general, a morphology of bars was developed in the samples identified as E-1, E-2, E-6, E-7, and E-8. In the samples E-3, E-4, E-5, E-8, and E-9, agglomerates of semi-spherical and flake-like particles were observed as well as the bars (see Fig. 2). At higher concentrations of zinc acetate (≥0.1 M), the morphology of particles takes the shape of bars with the exception of sample 8, which had the two types of morphologies. This situation could be associated with a transition point between the two types of morphologies. As the concentration of the zinc acetate decreased, the formation of agglomerates of particles with different morphology prevailed. In this sense, the samples E-3 and E-4 developed agglomerates of semi-spherical particles with a notable compaction, unlike the sample E-9 where a smaller grain boundary was observed. These results are consistent with those reported by Pacholski et al. who proposed a preferential growth through the z axis of the wurtzite crystalline structure of ZnO. They reported the formation of particles with the bar shape of ZnO when the concentration of zinc acetate was higher than 0.1 M (Pacholski et al. 2002). Likewise, an increase in the concentration of zinc acetate, and consequently of organic ligand, prevents the contact between the crystal planes of the hexagonal structure of ZnO, promoting the anisotropic growth through z axis. Further, increasing the concentration of the zinc acetate leads to increase the saturation (S) of the medium, which causes a decrease in the value of critical radius ($r*$) required for that developed nuclei begin to grow. Under this condition, the particle growth is energetically favored due to that the formation of larger crystals that decrease their surface energy. In contrast, by using the lowest concentration of the zinc acetate (0.02 M), the formation of smaller particles is favored due to an increase in the critical radius as was mentioned.

Once the morphology of each ZnO sample was analyzed, the average particle size was calculated. For this purpose, 100 ZnO particles of each sample were measured and the average particle size was obtained. With regard to the morphology of bar shape, the lowest particle size corresponded with the sample E-2, which presented an average length in their bars of 130 nm. On the contrary, the sample E-7 developed the longer bars of about of 200 nm.

Photocatalytic activity

The photocatalytic activity of the ZnO samples synthesized according to the factorial design was evaluated in the photo-oxidation reaction of nitric oxide in air. A typical experiment was performed with a mass of 50 mg of photocatalyst dispersed in an area of 0.08 m^2 and using an initial NO concentration of 1 ppm with a content of H_2O vapor minor than 0.4 ppm. Figure 3 shows the NO conversion degree (%) reached after 2 h of UV irradiation using as photocatalyst the
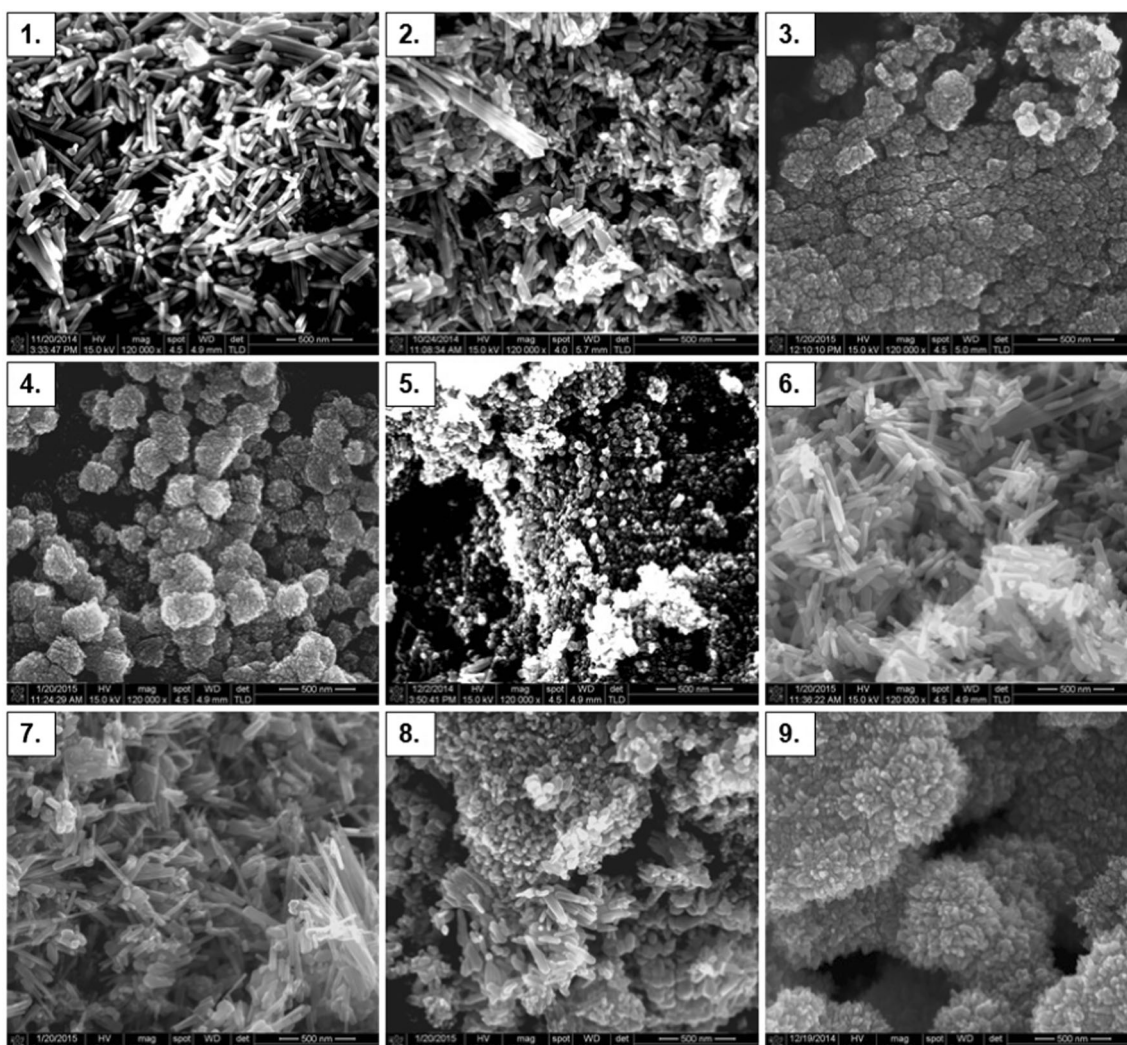
Fig. 2 SEM images of ZnO samples prepared by the sol-gel method

nine ZnO samples obtained from the factorial design. For all the cases, the stationary state was reached in at least 30 min. A
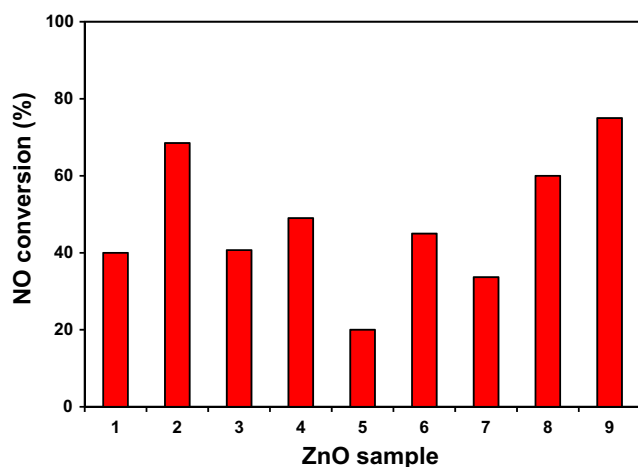

Fig. 3 NO conversion using the ZnO samples as photocatalyst after 2 h of irradiation (m = 50 mg, Q = 1 L·min^{-1}, I = 8.2 W·m^{-2})

strong influence of the experimental conditions of synthesis over the NO conversion degree was observed due to the physical properties developed in each ZnO sample. As an indicative of the importance of experimental conditions of synthesis in the NO conversion degree, it was observed that these values ranged from 75 (E-9) to 20 % (E-5). In general, no morphology was considerably better than the other to determine a high photocatalytic activity in ZnO. Although the samples showed similar values of specific surface area in the series of samples with spherical morphology, the sample E-9 showed a notably high activity. On the other hand, when were tested samples of ZnO with morphology of bars as photocatalysts, these showed a higher activity as the length of its particles was smaller. In this case, a short length from the site of the generation of the electron hole pair to the ZnO surface allows an easy transfer of the charges. Based on the analysis of the photocatalytic activity of the nine ZnO samples and its relation with the morphology and surface area, it seems to be clear that another parameter should act in an important way to improve the

photocatalytic activity of the samples. This situation will be discussed later.

Figure 4 shows the profile of the evolution of the NO conversion degree since the beginning of the photocatalytic reaction until the system has reached the stationary state, for the samples with the highest (E-9) and lowest photocatalytic activity (E-5). The difference between the two photocatalytic activities may be associated with several factors, but due to the amount of sample used in both experiments (50 mg in 0.08 m^2), the adsorption was an important factor in the NO conversion degree. In this sense, the adsorption of more NO molecules was favored in the sample E-9, which has twice the surface area than the sample E-5. Then, a higher surface area favors the adsorption of the NO molecule in the active sites of photocatalyst and increases the efficiency of the photocatalytic process.

Based on the obtained results with the nine samples of ZnO, the software provided a mathematical model considering the NO conversion degree as response (equation 2).

$$NO \text{ conversion } (\%) = 41.6 + 1.27A + 78B - 16.8AB \quad (2)$$

Where A represents the concentration of NH_4OH (M) and B corresponds to the concentration of zinc acetate (M). Considering the mathematical model, the equation (2) determines as optimal values of synthesis when $A = 0.8$ M and $B = 0.2$ M (sample E-8) to obtain the best photocatalyst. However, when this combination was used in experimental values to prepare ZnO, the NO conversion degree reached was only 60 %. The difference between the values obtained experimentally and by the equation (2) was about 30 % (see Fig. 5). This difference can be due to several factors. The first one is that the number of experiments could be low. In the same way, there is an experimental error associated with the dispersion degree of the photocatalysts on the glass substrate. Additionally, the model does not take into account the
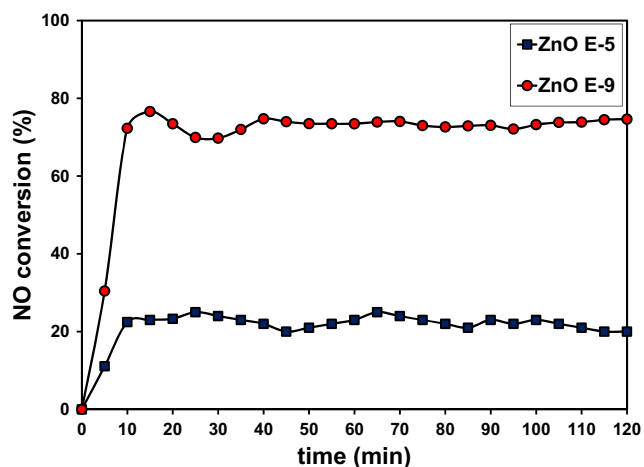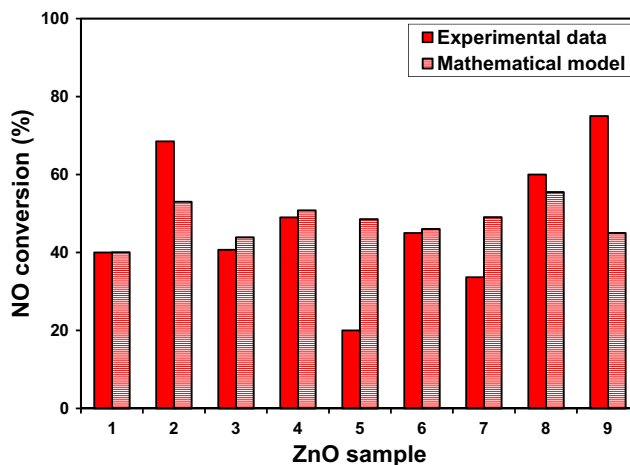

Fig. 5 Comparison of NO conversion values (%) obtained from experimental data and using equation (6) when TiO_2 was employed as photocatalyst

transition in morphology of ZnO samples. To check this point, the ZnO samples with the lowest (E-5) and highest (E-9) photocatalytic activity were analyzed by transmission electron microscopy (TEM) and high resolution transmission electron microscopy (HRTEM) in order to correlate their respective activities with its morphology and the preferential orientation of the crystalline planes. Figure 6a shows the morphology of the sample E-5, which consisted of a mixture of particles with shapes of polyhedral and bars, not observed previously by the SEM analysis. The average particle size calculated from TEM analysis, 61 nm, was very similar to that obtained from Scherrer equation. Moreover, as is shown in Fig. 6b, the sample E-9 formed by bean-like particles with an average size of 14 nm had a value significantly less than the calculated from the SEM images and Scherrer equation for the sample. The difference between the particle size values obtained by TEM and SEM lies in the difficulty of measuring particles smaller than 20 nm due to their agglomeration. Some images were taken at HRTEM to identify crystal planes in E-5 and E-9. Figure 6c, d shows the crystallographic planes (100), (002), and (101) in the sample E-5. In a recurrent way, the crystalline plane (100) appeared in different zones of the sample. On the other hand, an analysis in several ZnO particles of sample E-9 revealed a preferential orientation of the crystalline plane (002; Fig. 6e, f). Thus, the difference of photocatalytic activity between the samples E-5 and E-9 may be too associated with the crystallographic orientation of the planes exposed in the surface. The sample E-9 developed a preferential orientation of its particles in the plane (002), which according to the literature has the highest photocatalytic activity in the ZnO hexagonal structure (Li et al. 2008). The crystalline plane (002) is formed in one side of zinc atoms which promotes the adsorption of OH$^-$ ions due to the positive charge of the zinc, which gives polarity in the sample E-9. In this context, the polarity of the sample can be corroborated by the relationship between the intensities of planes (002) and (100) from the

Fig. 4 Evolution of NO conversion using the samples 5 and 9 of ZnO as photocatalyst ($m = 50$ mg, $Q = 1$ L·min^{-1}, $I = 8.2$ W·m^{-2})

Fig. 6 TEM images of representatives ZnO samples: **a** 5 and **b** 9. HRTEM images of the samples: **c**, **d** E-5 and **e**, **f** E-9
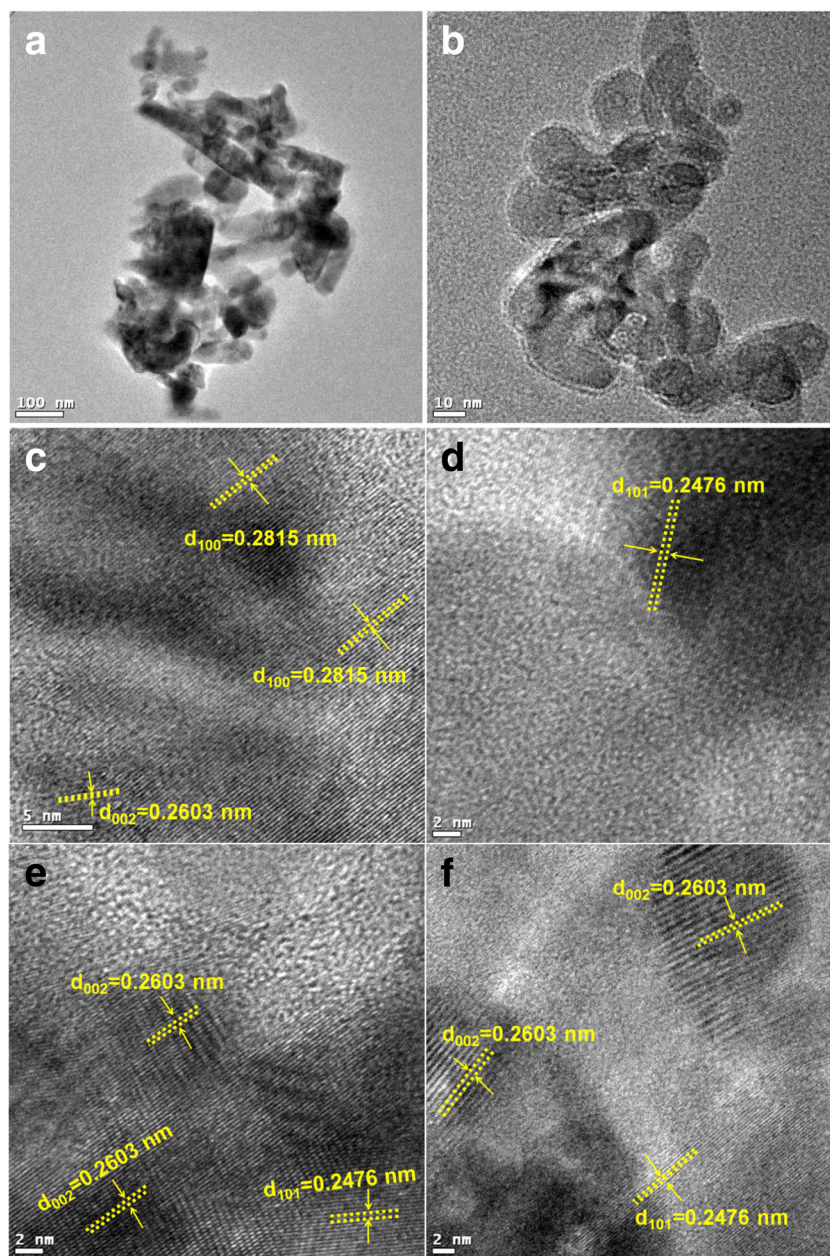
difractogram. The relation of these intensities for the samples E-5 and E-9 were 1.0 and 1.2, respectively. A higher value of the relation (002)/(100) favored the formation of OH$^{\bullet}$ radicals, which participate in the oxidation reaction of nitric oxide.

Effect of the mass of photocatalyst in the NO conversion

According to the experimental results, the sample E-9 was selected for subsequent experiments due to its highest NO conversion degree (75 %) when used as photocatalyst. In order to determine the effect of the mass of photocatalyst in the NO conversion degree, two additional experiments were performed with 100 and 200 mg of photocatalyst. Figure 7a shows that the highest NO conversion degree (94 %) was

reached using a mass of 200 mg after 2 h. When 100 mg of photocatalyst was employed, it reached a conversion degree of 85 %, and when the mass of photocatalyst decreased to 50 mg, the conversion decreased to 75 %. A commercial ZnO (ZnO-com) was also evaluated for comparative purposes with the sample E-9. As is shown in Fig. 7b, a higher NO conversion degree was reached when 100 and 200 mg (>95 %) were used with respect to the values observed in E-9. However, when 50 mg of ZnO-com was used, it was observed that there was an evident deactivation of the oxide during the course of the reaction.

Additional experiments were performed using the commercial oxide TiO$_2$ (Degussa, P-25). When 100 and 200 mg of the TiO$_2$ P-25 were used as a photocatalyst, a high NO conversion
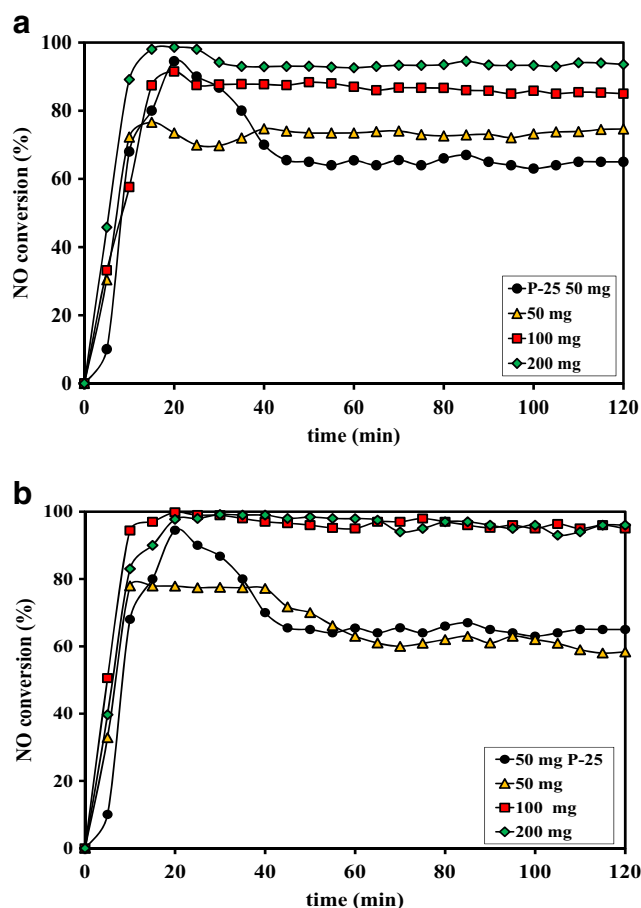
Fig. 8 NO conversion using the ZnO sample E-9 as photocatalyst under 70 %RH ($Q = 1$ L·min^{-1}, $I = 8.2$ W·m^{-2})

minor than 0.4 ppm, it is significantly taken into account that it is of the same order with the initial concentration of NO in a typical experiment (1 ppm). Therefore, some experiments were done to analyze the effect of the relative humidity in the NO conversion degree. Figure 8 shows the evolution of the NO conversion degree using ZnO E-9 as photocatalyst in an experiment with 70 % RH. It can be seen that an increase in the relative humidity decrease the photocatalytic activity of the ZnO sample. In the first 20 min of irradiation, the conversion was higher compared with the experiment performed with <0.4 ppm of H_2O. However, the deactivation of the photocatalyst was evident at longer reaction times when the reaction was carried out with 70 % RH. This can be explained from the fact that the ZnO surface is hydrophobic at first, but its illumination tends to be hydrophilic as a consequence of the interaction of the adsorbed oxygen and electrons in the conduction band of ZnO. This situation promotes the H_2O adsorption and increases the competition for the adsorption sites between NO and H_2O molecules. This phenomenon is directly proportional with the amount of radiation over the

Fig. 7 NO conversion employing different mass of the ZnO sample: a ZnO-com and b E-9 ($Q = 1$ L·min^{-1}, $I = 8.2$ W·m^{-2})

was observed (>97 %). However, for 50 mg of TiO_2 P-25, the tendency of the evolution of NO conversion was similar to the ZnO commercial. The NO conversion in steady state using TiO_2 P-25 as photocatalyst was 65 %, which is 12 % higher than the observed commercial ZnO. Nevertheless, the sample ZnO E-9 showed a higher photocatalytic activity in comparison with the commercial ZnO and TiO_2 photocatalysts when a low mass (50 mg) of photocatalyst was applied. This implies that under drastic operating conditions of the photocatalyst, such as a high NO concentration or long exposure, the sample E-9 has a better performance than the commercial oxides. The origin of the difference of photocatalytic activity between the samples may be associated with its physical properties (see Table 2).

Effect of the relative humidity in the NO conversion degree

The relative humidity (RH) is a factor that can influence in a reaction carried out in gaseous phase. Until this point, the experiments were performed only in the presence of residual H_2O vapor in the air used as carry gas. Although this value is
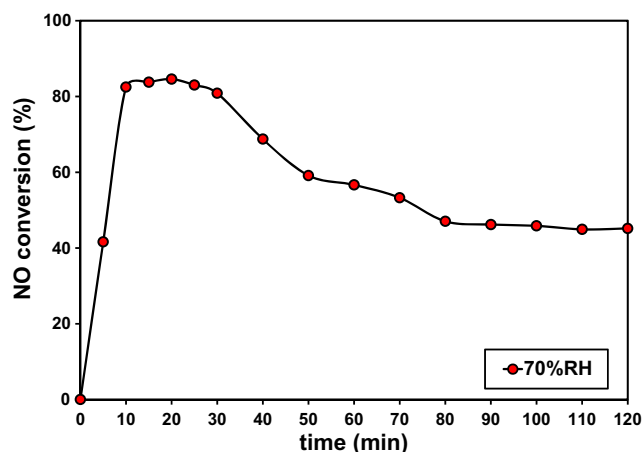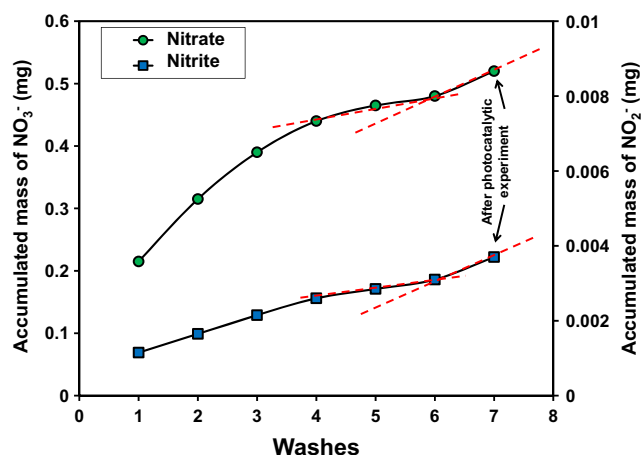

Fig. 9 Accumulated mass of nitrate and nitrite ions extracted from the ZnO sample E-9

Table 3 Experiments of NO photooxidation

Operating conditions	NO conversion (%)	Conversion NO → NO_3^- (%)	Conversion NO → NO_2^- (%)
1 ppm; 1 L·min^{-1}; 8.2 W·m^{-2}; <0.4 ppm H_2O	81	52	1.1
1 ppm; 1 L·min^{-1}; 8.5 W·m^{-2}; <0.4 ppm H_2O	87	52	2.7
1 ppm; 1 L·min^{-1}; 10.1 W·m^{-2}; <0.4 ppm H_2O	93	63	0.1
1 ppm; 1 L·min^{-1}; 8.2 W·m^{-2}; 70 %RH	71	86	5.0

surface of ZnO (Sun et al. 2001). Despite that there is a higher amount of H_2O molecules adsorbed on the ZnO surface, this apparently does not contribute to the photocatalytic process by the generation of a larger amount of OH$^\bullet$ radicals. This may indicate that the mechanism of the NO photooxidation in the presence of ZnO is preferably carried out by a direct oxidation of NO by the holes generated during the photocatalytic process or by the participation of the superoxide radical generated in the conduction band of the photocatalyst. However, this situation should be reviewed in more detail.

Analysis of reaction products

The ZnO powders used as photocatalyst were washed and sonicated in 50 mL of deionized water to identify and quantify the nitrate ions (NO_3^-) and nitrite ions (NO_2^-) formed as a product of the advanced oxidation of NO. The formation of nitrate and nitrite ions was quantified in some photocatalytic experiments that were carried out under the conditions of $Q = 1$ L·min^{-1}, 1 ppm of NO, <0.4 ppm H_2O, and 70 % RH, and with an irradiance of 8.2, 8.5, and 10.1 W·m^{-2}.

Prior to the photocatalytic experiments, the photocatalyst was washed several times in order to detect nitrates and nitrites from the synthesis step. Figure 9 shows that in the first wash, the sample E-9 had a significant amount of nitrate and nitrite ions being 0.22 and 0.001 mg, respectively. The extracted amount of the ions is considerably higher than the theoretical amount according with conditions of the photocatalytic experiment, where a 100 % of NO conversion to NO_3^- would produce only 0.1 mg. This confirmed the presence of nitrate ions as an impurity in high concentration in the material matrix and revealed that an efficient washing was required in order to eliminate interferences with the results from the photocatalytic experiment. Figure 9 shows the accumulative mass extracted of NO_3^- and NO_2^- ions in each case for six consecutive washings of photocatalyst. After the sixth wash, the accumulated mass of NO_3^- ions increased only at 3 %, so it was taken as a reference point for considering the sample free of nitrate and nitrites ions. Therefore, after six washing cycles of the sample E-9 of ZnO, it was dried and was used as a photocatalyst in the oxidation reaction of NO, and then the reaction products were

analyzed. According to the results, the accumulated mass of nitrate and nitrite ions increased in the seventh wash. This was associated with the presence of oxidation products of the NO molecule under the conditions described previously. Here, the conversion of NO to NO_3^- and NO_2^- ions was 52 and 1 %, respectively. The results are listed in Table 3.

Additionally, two photocatalytic experiments were carried out increasing the average irradiance of the reactor at 8.5 and 10.1 W·m^{-2}. The nitrate ion analysis of these experiments revealed an increase in the selectivity of the photooxidation of NO to NO_3^- when the photocatalyst was irradiated with 10.1 W·m^{-2}. From the results in Table 3, it can be concluded that at the same level of humidity (<0.4 ppm H_2O), the selectivity of the conversion reaction of NO to NO_3^- increases as the irradiance increases. Under 10.1 W·m^{-2} of irradiance, the selective conversion of NO_3^- was 63 %. Meanwhile, at a constant value of irradiance, $I = 8.2$ W·m^{-2}, the selectivity in the conversion of NO to NO_3^- increased significantly when the reaction was performed with 70 % RH. Under this condition, the conversion of NO to NO_2^- was 5 % and up to 86 % in a conversion to NO_3^-. In general, the results indicate that while an increase in the relative humidity leads to a slight decrease in the NO conversion, it promotes a high selectivity towards nitrate ion formation.

Conclusions

ZnO samples were prepared successfully by sol-gel applying a factorial design of the type 3^n ($n = 2$). As a direct consequence of modifying two experimental variables of synthesis, the physical properties of ZnO samples were strongly influenced and they led to the formation of samples with different photocatalytic activity. In particular, the concentration of zinc acetate played the most important role to obtain materials with higher surface area, and consequently, higher photocatalytic activity for the photooxidation reaction of NO. In addition, the sample with the highest photocatalytic activity showed also a preferential orientation in the crystalline plane (002), which is associated with a high activity due to the adsorption of large amounts of hydroxyl ions. Although a good correlation was

observed between the values of NO conversion degree predicted by the mathematical model and the obtained experimentally, some differences were observed. This situation was associated with some physical properties not considered in the mathematical model, i.e., the different morphologies observed in the ZnO samples, and preferential orientation of the crystalline planes exposed to the surface of photocatalyst. The presence of reaction products was successfully confirmed. In general, an increase in the humidity and the irradiance had a positive effect in the selective oxidation of NO to NO_3^- ions. Finally, according to the results, it was confirmed that NO_3^- ions was the main product of the NO photooxidation reaction.

References

Bacaksiz E, Parlak M, Tomakin M, Özcelik A, Karakiz M, Altunbas M (2009) The effects of zinc nitrate, zinc acetate and zinc chloride precursors on investigation of structural and optical properties of ZnO thin films. J Alloys Compd 466(1–2):447–450. doi:10.1016/j.jallcom.2007.11.061

Baruah S, Dutta J (2009) Hydrothermal growth of ZnO nanostructures. Sci Tech Adv Mater 10:1–19. doi:10.1088/1468-6996/10/1/013001

Bloh JZ, Folli A, Macphee DE (2014) Photocatalytic NO$_x$ abatement: why the selectivity matters. RSC Adv 4:45726–45734. doi:10.1039/c4ra07916g

Cademartiri L, Ozin GA (2010) Emerging strategies for the synthesis of highly monodisperse colloidal nanostructures. Phil Trans R Soc A 368:4229–4248. doi:10.1098/rsta.2010.0126

Condon JB (2006) Surface area and porosity determinations by physisorption. Elsevier, Amsterdam

García Núñez C, Pau JL, Ruíz E, García Marín A, García BJ, Piqueras J, Shen G, Wilbert DS, Kim SM, Kung P (2014) Enhanced fabrication process of zinc oxide nanowires for optoelectronics. Thin Solid Films 555:42–47. doi:10.1016/j.tsf.2013.12.011

Hu G, Guo W, Yu R, Yang X, Zhou R, Pan C, Wang ZL (2016) Enhanced performances of flexible ZnO/perovskite solar cells by piezo-phototronic effect. Nano Energy 23:27–33. doi:10.1016/j.nanoen.2016.02.057

Huang Y, Guo C, Huang L, Dong Q, Yin S, Sato T (2013) Photocatalytic oxidation of NO$_x$ gases using ZnO with superstructure by a low temperature soft solution process. Int J Nanotechnol 10(1–2):30–37. doi:10.1504/IJNT.2013.050878

Kontopoulou I, Angelopoulou A, Bouropoulos N (2016) ZnO spherical porous nanostructures obtained by thermal decomposition of zinc palmitate. Mater Lett 165:87–90. doi:10.1016/j.matlet.2015.11.110

Kowsari E, Bazri B (2014) Synthesis of rose-like ZnO hierarchical nanostructures in the presence of ionic liquid/Mg^{2+} for air purification

Lasek J, Yu YH, Wu JCS (2013) Removal of NO$_x$ by photocatalytic processes. J Photochem Photobiol C: Photochem Rev 14:29–52. doi:10.1016/j.jphotochemrev.2012.08.002

Li GR, Pan GL, Yan TY, Gao XP, Zhu HY (2008) Morphology–function relationship of ZnO: polar planes, oxygen vacancies, and activity. J Phys Chem C 112(31):11859–11864. doi:10.1021/jp8038626

Luévano-Hipólito E, Martínez-de la Cruz A. (2016) Sol-gel synthesis and photocatalytic performance of ZnO toward oxidation reaction of NO. Res Chem Intermed 42:4879–4891. doi:10.1007/s11164-015-2327-4

Lyu J, Zhu L, Burda C (2014) Considerations to improve adsorption and photocatalysis of low concentration air pollutants on TiO$_2$. Catal Today 225:24–33. doi:10.1016/j.cattod.2013.10.089

Moezzi A, McDonagh AM, Cortie MB (2014) Zinc oxide particles: synthesis, properties and applications. Chem Eng J 185-186:1–22. doi:10.1016/j.cej.2012.01.076

Nakata K, Fujishima A (2012) TiO$_2$ photocatalysis: design and applications. J Photochem Photobiol C: Photochem Rev 13:169–189. doi:10.1016/j.jphotochemrev.2012.06.001

Pacholski C, Kornowski A, Weller H (2002) Self-assembly of ZnO: from nanodots to nanorods. Angew Chem Int Ed 41(7):1188–1191. doi:10.1002/1521-3773(20020402)41:7<1188::AID-ANIE1188>3.0.CO;2-5

Pei CC, Leung WW (2014) Solar photocatalytic oxidation of NO by electrospun TiO$_2$/ZnO composite nanofiber mat for enhancing indoor air quality. J Chem Technol Biotechnol 89(11):1646–1652. doi:10.1002/jctb.4506

Peng X, Wickham J, Alivisatos AP (1998) Kinetics of II-VI and III-V colloidal semiconductor nanocrystal growth: "focusing" of size distributions. J Am Chem Soc 120(21):5343–5344. doi:10.1021/ja9805425

Radzimska AK, Jesionowsky T (2014) Zinc oxide-from synthesis to application: a review. Materials 7:2833–2881. doi:10.3390/ma7042833

Sun R, Nakajima A, Fijishima A, Watanabe T, Hashimoto K (2001) Photoinduced surface wettability conversion of ZnO and TiO2 thin films. J Phys Chem B 105(10):1984–1990. doi:10.1021/jp002525j

Takeuchi M, Sakai S, Ebrahimi A, Matsuoka M, Anpo M (2009) Application of highly functional Ti-oxide-based photocatalysts in clean technologies. Top Catal 52:1651–1659. doi:10.1007/s11244-009-9300-7

Toma FL, Bertrand G, Klein D, Coddet C (2004) Photocatalytic removal of nitrogen oxides via titanium dioxide. Environ Chem Lett 2:117–121. doi:10.1007/s10311-004-0087-2

Verbruggen SW (2015) TiO$_2$ photocatalysis for the degradation of pollutants in gas phase: from morphological design to plasmonic enhancement. J Photochem Photobiol C: Photochem Rev 24:64–82. doi:10.1016/j.jphotochemrev.2015.07.001

Wei Y, Huang Y, Wu J, Wang M, Guo C, Dong Q, Yin S, Sato T (2013) Synthesis of hierarchically structured ZnO spheres by facile methods and their photocatalytic deNO$_x$ properties. J Hazard Mater 248-249:202–210. doi:10.1016/j.jhazmat.2013.01.012

Zhang M, Jin F, Zhen M, Liu J, Zhao Z, Duan X (2014) High efficiency solar cell based on ZnO nanowire array prepared by different growth methods. RCS Adv 4:10462–10466. doi:10.1039/C3RA47146B